2014 Spring

“Advanced Physical Metallurgy”

- Bulk Metallic Glasses -

05.08.2014

Eun Soo Park

Office: 33-313
Telephone: 880-7221
Email: espark@snu.ac.kr
Office hours: by appointment

4.6 Bulk Metallic Glass Casting Methods

4.6.1 Water-Quenching Method : CR~ about 10-100 K/s

4.6.2 High-Pressure Die Casting

: offer high solidification rates high productivity, low casting defect, and possible to produce more complex shapes even in alloys with a high viscosity

4.6.6 Squeeze-casting Method

: Push the molten alloy through hydraulic high pressure into the Cu mold until the liquid alloy completely solidified → Undercooling to much below the equilibrium solidification temperature

4.6.3 Copper Mold Casting : most common and popular method to produce BMGs

: Injection casting, Centrifugal casting, Strip casting, Arc melting, Suction casting, tilt-casting, Cap-cast technique (bringing a metallic cap into contact with the molten metal, and applied a small pressure of about 1 kN → high CR)

→ Automatic Production Process of BMGs (Human error ↓ & Homogeneity ↑)

4.6.8 Unidirectional Zone Melting Method

4.6.9 Electromagnetic Vibration Process

: destroy clusters of strong local order → GFA↑

4.8 Mechanical Alloying → Extrusion or Spark Plasma Sintering (multi-step process)

: used to easily produce amorphous phases in those systems where conventional melting and casting methods prove difficult or impossible (wide composition ranges)

4.7 Bulk Metallic Glass Composites

: exhibit much better mechanical properties → detail later in Chapter 8

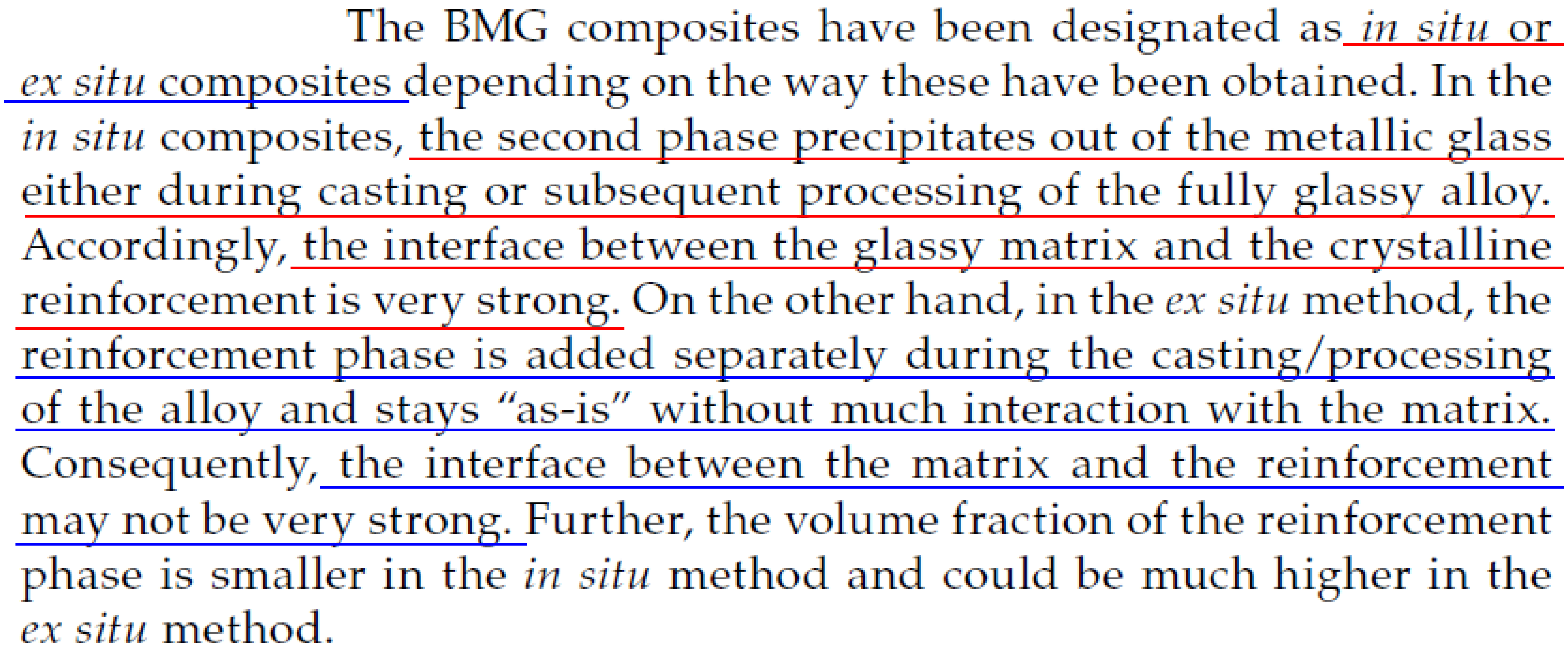

The BMG composites have been designated as *in situ* or *ex situ* composites depending on the way these have been obtained. In the *in situ* composites, the second phase precipitates out of the metallic glass either during casting or subsequent processing of the fully glassy alloy. Accordingly, the interface between the glassy matrix and the crystalline reinforcement is very strong. On the other hand, in the *ex situ* method, the reinforcement phase is added separately during the casting/processing of the alloy and stays "as-is" without much interaction with the matrix. Consequently, the interface between the matrix and the reinforcement may not be very strong. Further, the volume fraction of the reinforcement phase is smaller in the *in situ* method and could be much higher in the *ex situ* method.

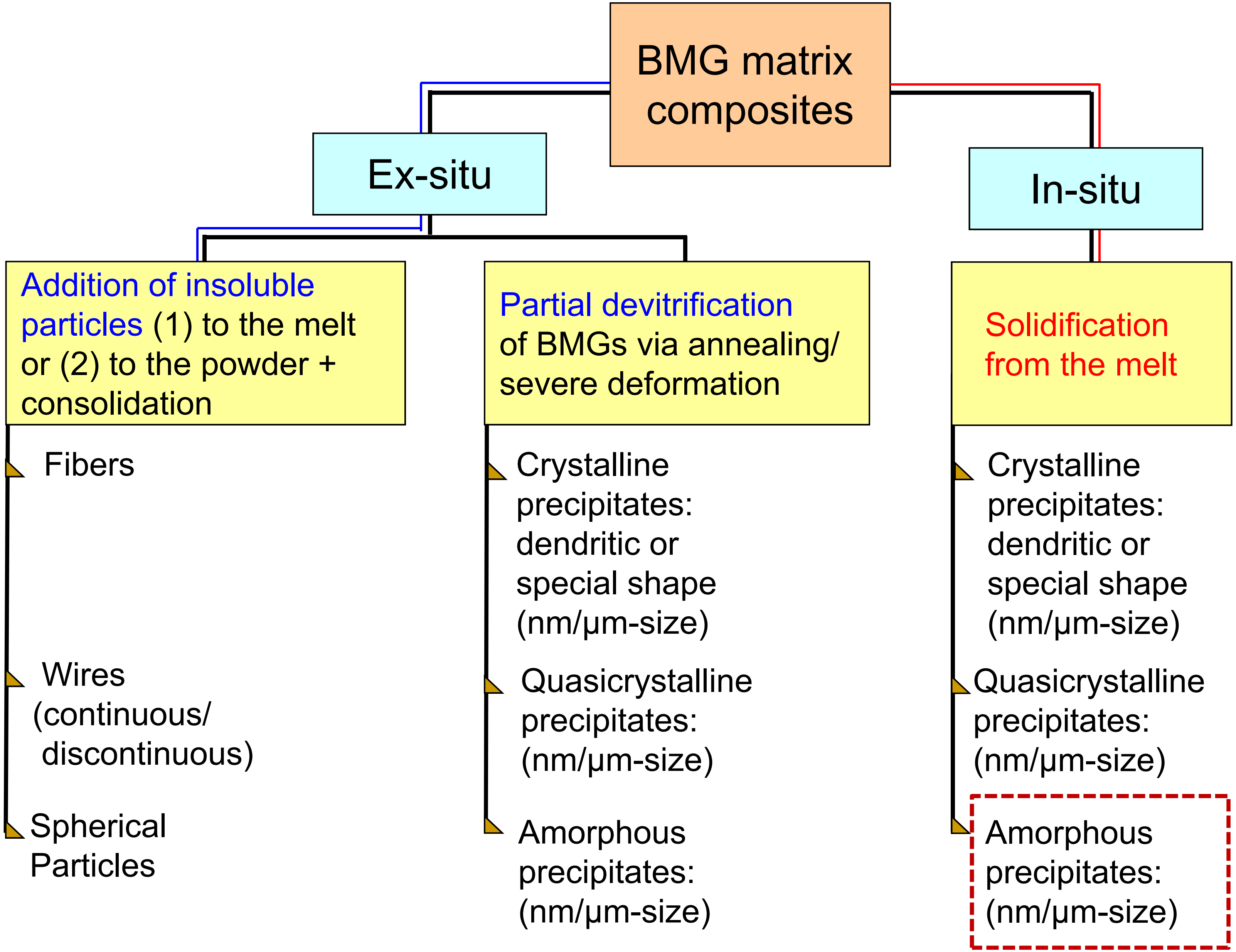

- BMG matrix composites
  - Ex-situ
    - Addition of insoluble particles (1) to the melt or (2) to the powder + consolidation
      - Fibers
      - Wires (continuous/ discontinuous)
      - Spherical Particles
    - Partial devitrification of BMGs via annealing/ severe deformation
      - Crystalline precipitates: dendritic or special shape (nm/µm-size)
      - Quasicrystalline precipitates: (nm/µm-size)
      - Amorphous precipitates: (nm/µm-size)
  - In-situ
    - Solidification from the melt
      - Crystalline precipitates: dendritic or special shape (nm/µm-size)
      - Quasicrystalline precipitates: (nm/µm-size)
      - Amorphous precipitates: (nm/µm-size)

Eckert at al, Adv Eng Mater 2007

IH4 Spinodal Decomposition?

In-situ Composite

*Formation of a composite microstructure within a **single production step***

a), b) Crystalline precipitates

c) Quasicystalline precipitates

d) Two phase amorphous composites

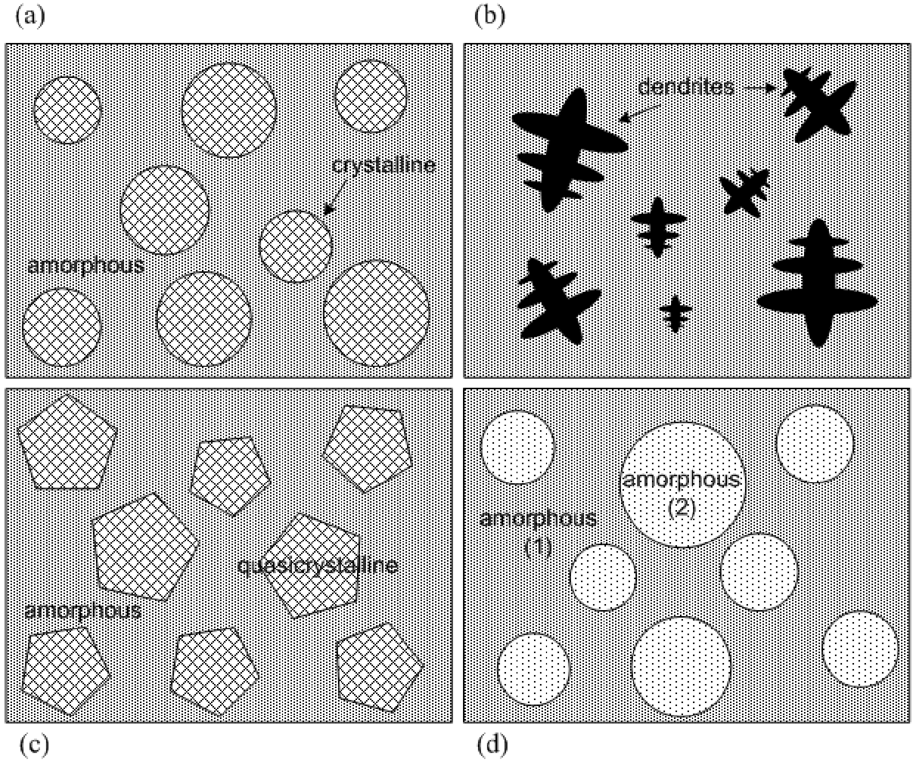

nature materials

NATURE MATERIALS | LETTER

Transformation-mediated ductility in CuZr-based bulk metallic glasses

S. Pauly, S. Gorantla, G. Wang, U. Kühn & J. Eckert

Affiliations | Contributions | Corresponding author

Nature Materials 9, 473–477 (2010) | doi:10.1038/nmat2767
Received 17 November 2009 | Accepted 09 April 2010 | Published online 16 May 2010

Figure 4: Schematic of the deformation process in the CuZr-based alloys investigated.

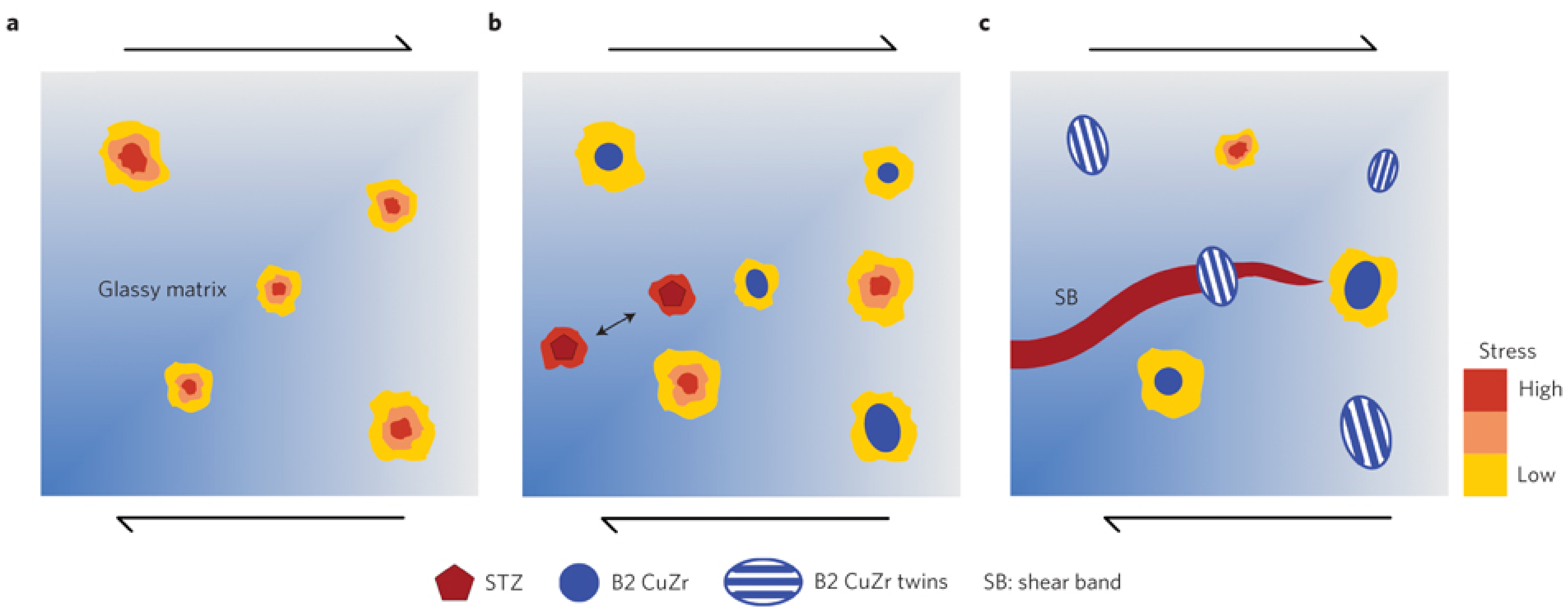

4.7.1 In Situ Composites: usually produced by adjusting the chemical composition of the alloy

: Shape of crystalline phase_usually dendritic → homogenized in the mushy (liquid+ soild) region_spherical shape → further improve the mechanical properties

1) Solidification : preciipitation of primary ductile phase

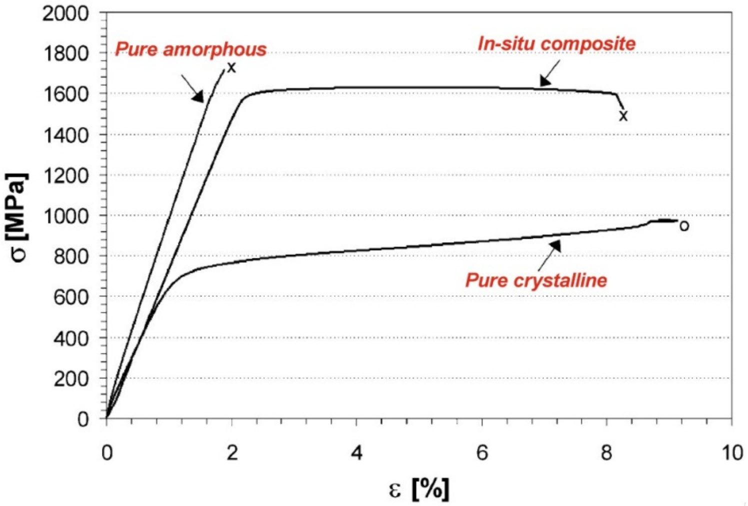

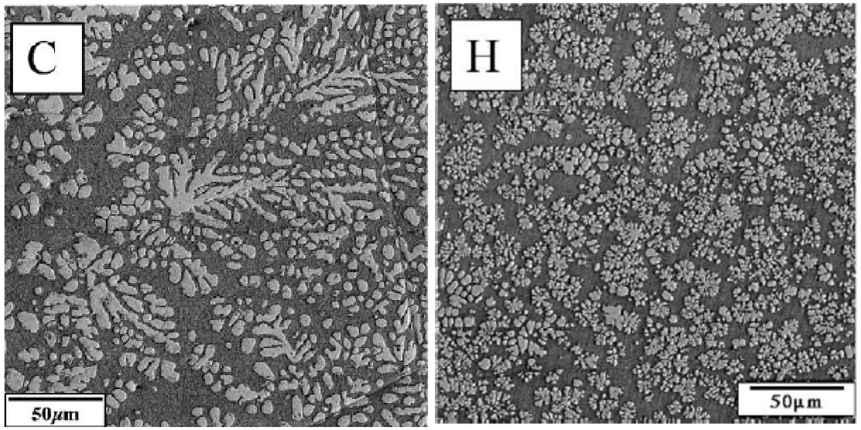

(Johnson et al., Acta Mater., 2001)

2) Solidification : precipitation of ductile phase

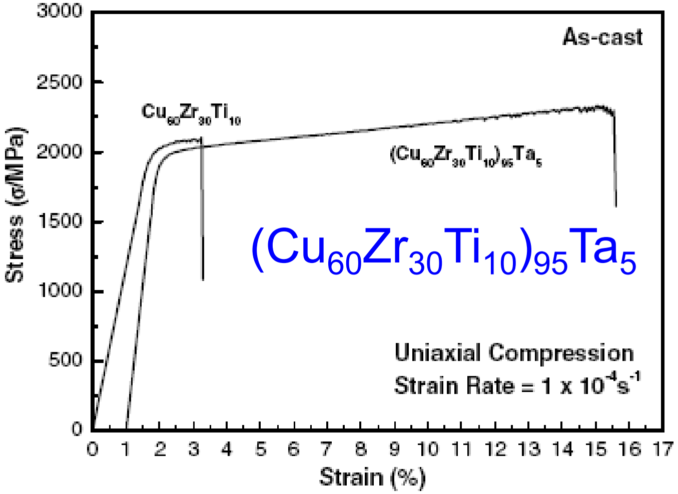

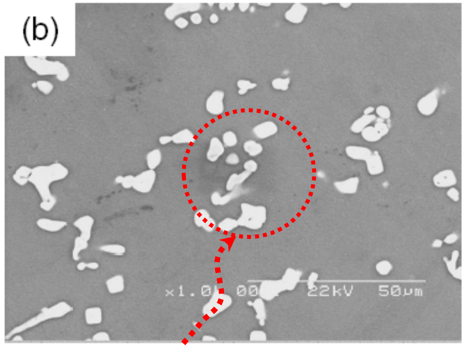

Ta rich particle

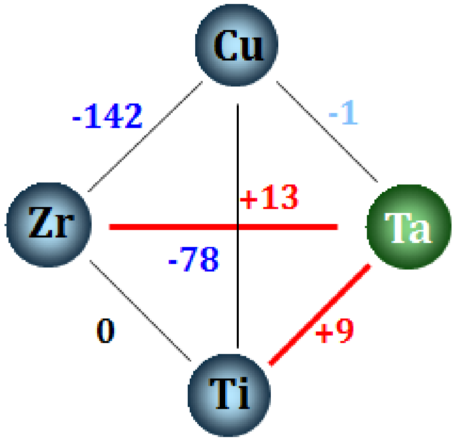

(Johnson et al., Acta Mater., 2001)

MATERIALS SCIENCE

Shape Memory Bulk Metallic Glass Composites

Douglas C. Hofmann

Glass-forming and shape memory metals may provide a route to fabricating materials with enhanced mechanical properties.

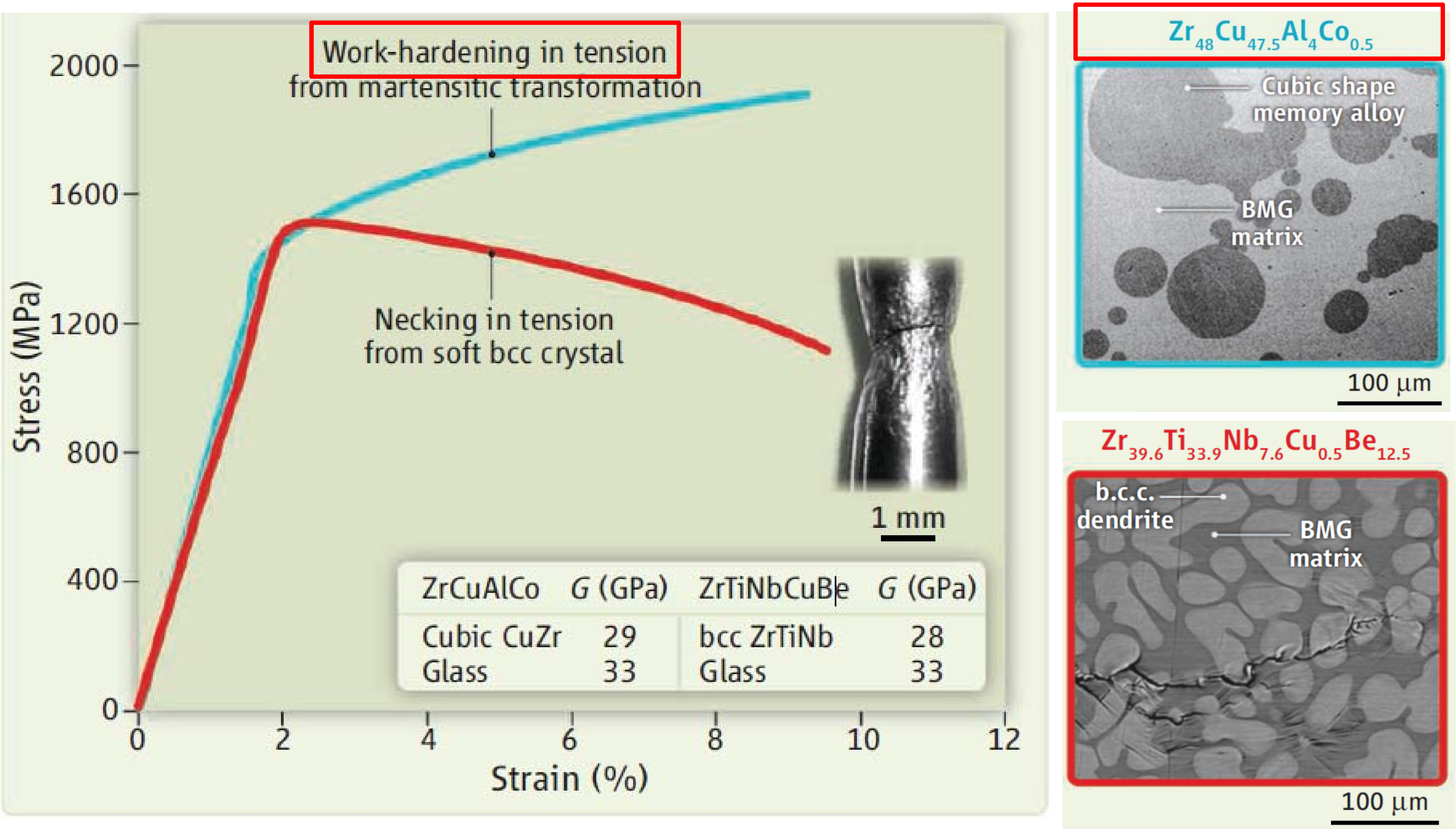

ZrCuAlCo	*G* (GPa)	ZrTiNbCuBe	*G* (GPa)
Cubic CuZr	29	bcc ZrTiNb	28
Glass	33	Glass	33

Douglas C. Hofmann, SCIENCE VOL 329 10 SEPTEMBER 2010

4.7.2 Ex Situ Composites: usually very large volume fraction of second crystalline phase

_ type of reinforcements_pure metals (tungsten, molybdenum, tantalum, nickel, copper and titanium), alloys (1080 steel, stainless steel, and brass), and non-metallics (SiC, diamond, and graphite)

For example: Melt-infiltration technique for the case of long and continuous fibers

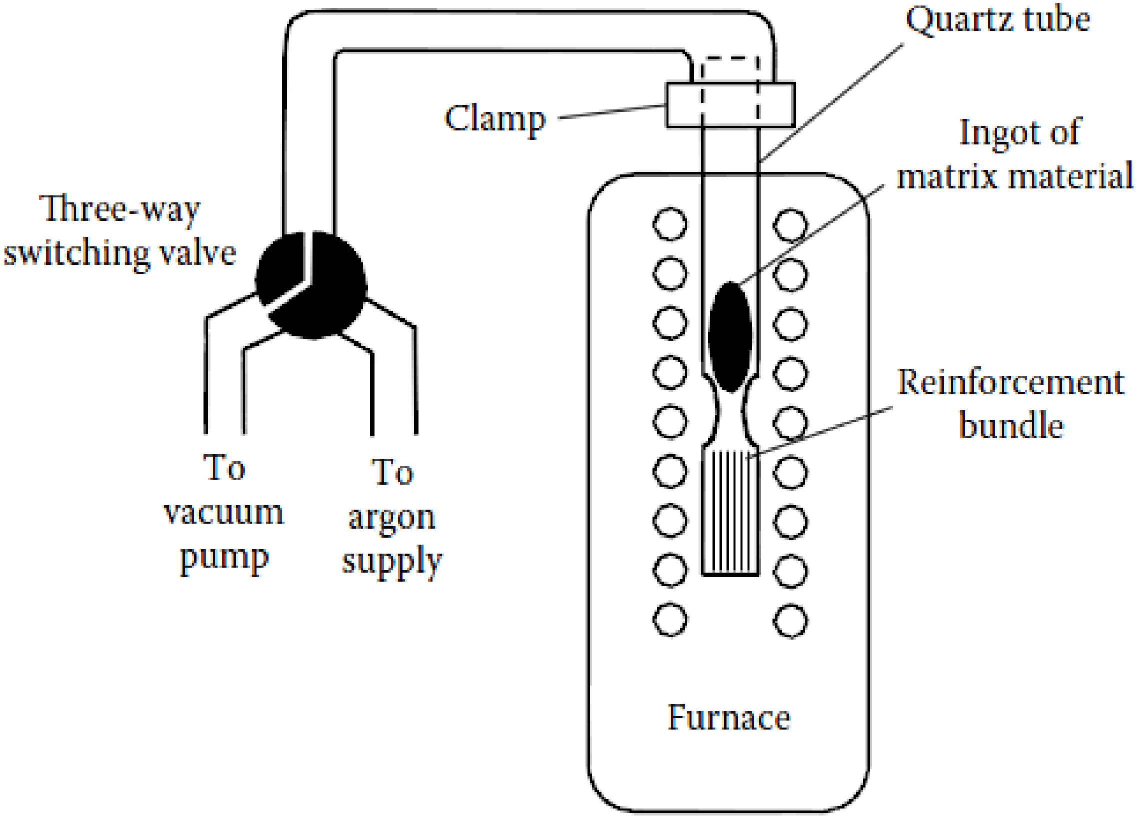

FIGURE 4.14
Schematic of the melt infiltration casting technique to produce *ex situ* BMG composites. (Reprinted from Dandliker, R.B. et al., *J. Mater. Res.*, 13, 2896, 1998. With permission.)

1) Casting : hard/ductile particle

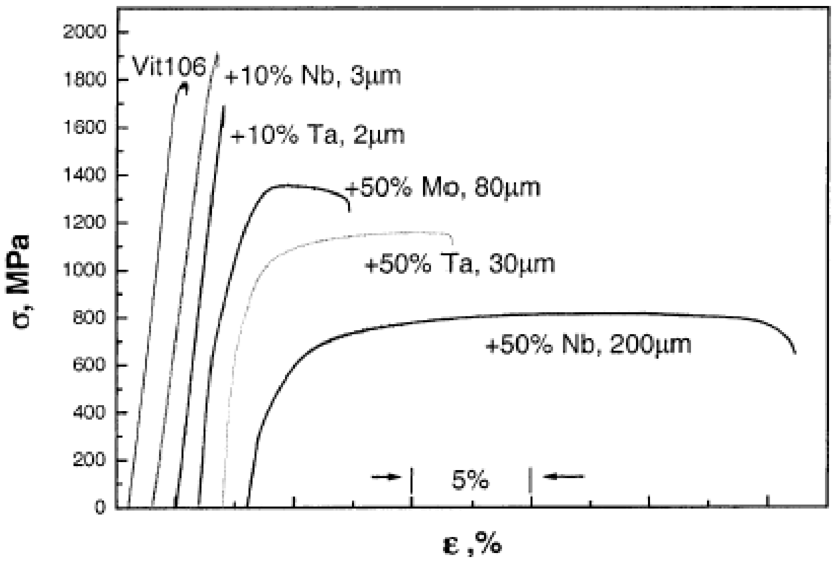

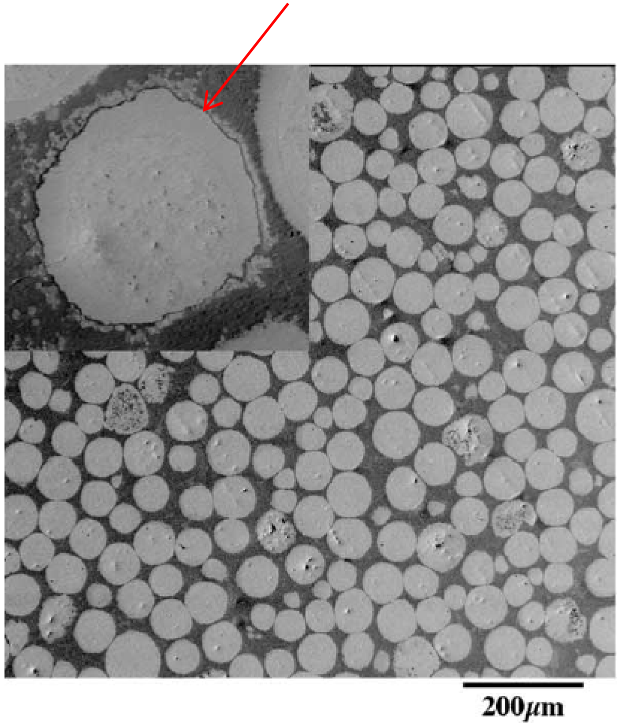

(Johnson et al., Acta Mater.,1999)

2) Extrusion : ductile powder

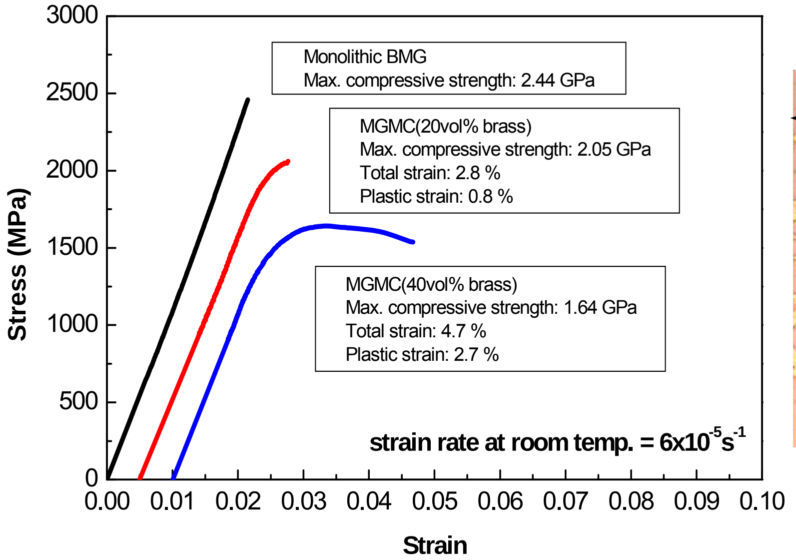

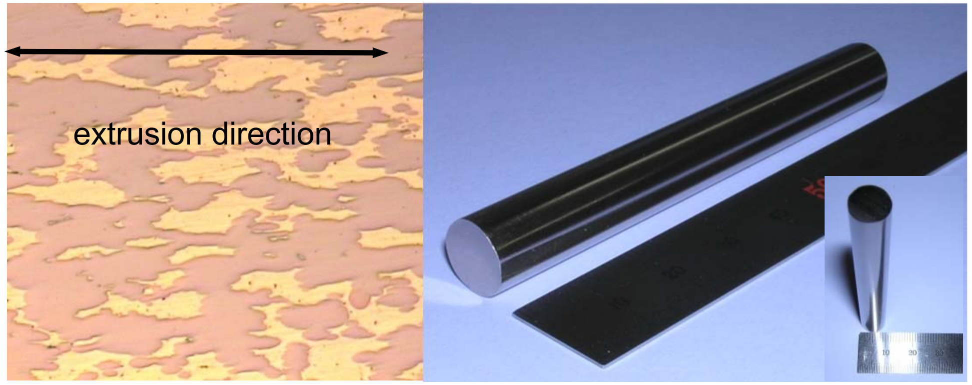

(Kim et al., J. Non-cryst. Solids, 2002)

4.9 Bulk Metallic Glass Foams

: have interesting combination of properties such as high stiffness in conjunction with very low specific weight, high gas permeability combined with high thermal conductivity, high mechanical energy absorption, and good acoustic damping.

→ Pores as a gaseous second phase_equally effective in inhibiting catastrophic failures resulting from shear band localization

Pore sizes ranging from the sub-micrometer to the millimeter scale and porosities ranging from 2% to more than 85%

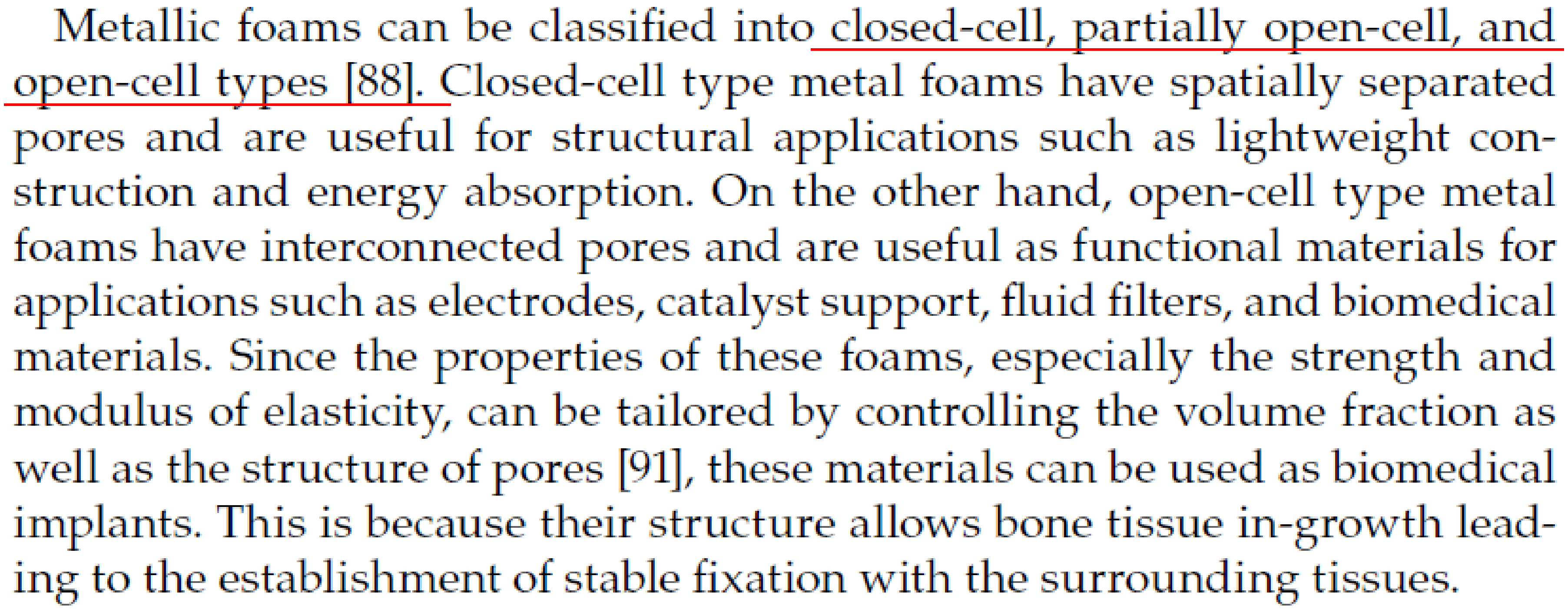

Metallic foams can be classified into closed-cell, partially open-cell, and open-cell types [88]. Closed-cell type metal foams have spatially separated pores and are useful for structural applications such as lightweight construction and energy absorption. On the other hand, open-cell type metal foams have interconnected pores and are useful as functional materials for applications such as electrodes, catalyst support, fluid filters, and biomedical materials. Since the properties of these foams, especially the strength and modulus of elasticity, can be tailored by controlling the volume fraction as well as the structure of pores [91], these materials can be used as biomedical implants. This is because their structure allows bone tissue in-growth leading to the establishment of stable fixation with the surrounding tissues.

Review of the state of the art in the processing of BMG foams I

- $Pd_{43}Cu_{27}Ni_{10}P_{20}$: produced by expansion in the liquid alloy of water vapor bubbles generated from hydrated boron oxide flux powders, followed by quenching.

First porous amorphous metal (2003)
~85 vol%, 200-1000 μm

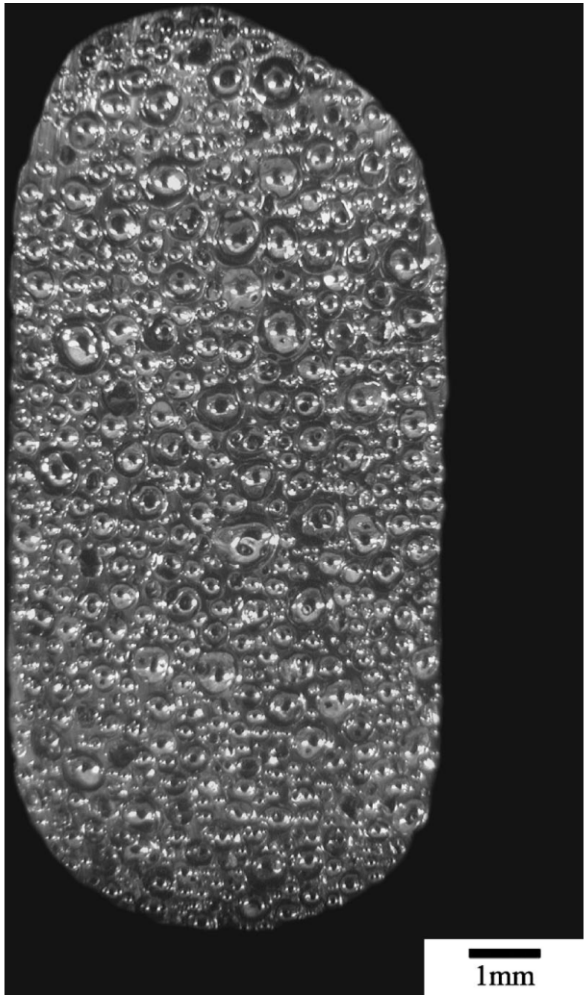

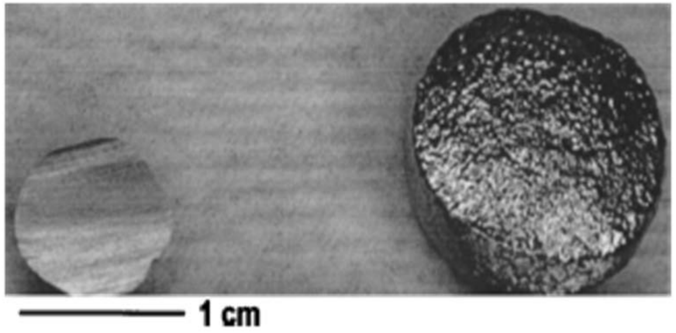

FIG. 11. Size comparison of $Pd_{43}Ni_{10}Cu_{27}P_{20}$ prefoam (left) and expanded foam (right) by rf-coil. The bubble volume fraction of the prefoam is 10%, while that of the final foam is 75%.

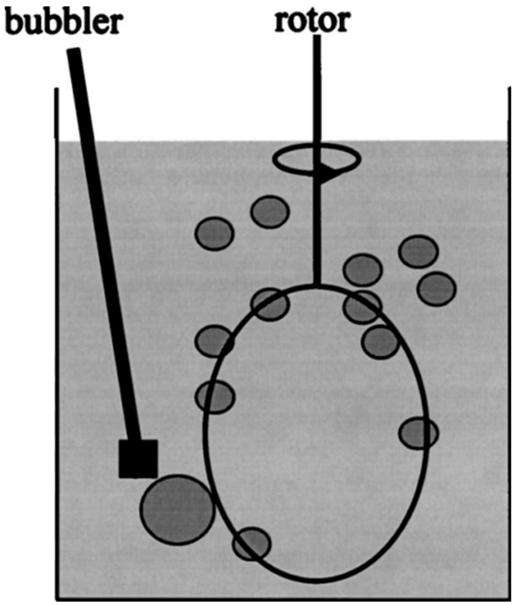

Schematic drawing of the eggbeater constructed for the mechanical air-entrapment method.
The setup comprises a molybdenum brush of 3 cm diameter spinning at speeds of up to 2500 rpm.

Review of the state of the art in the processing of BMG foams II

- **Wada and Inoue → open-cell structures**

(2003) by casting $Pd_{42.5}Cu_{30}\ Ni_{7.5}P_{20}$ into beds of NaCl particles, quenching, and removing the salt by dissolution.

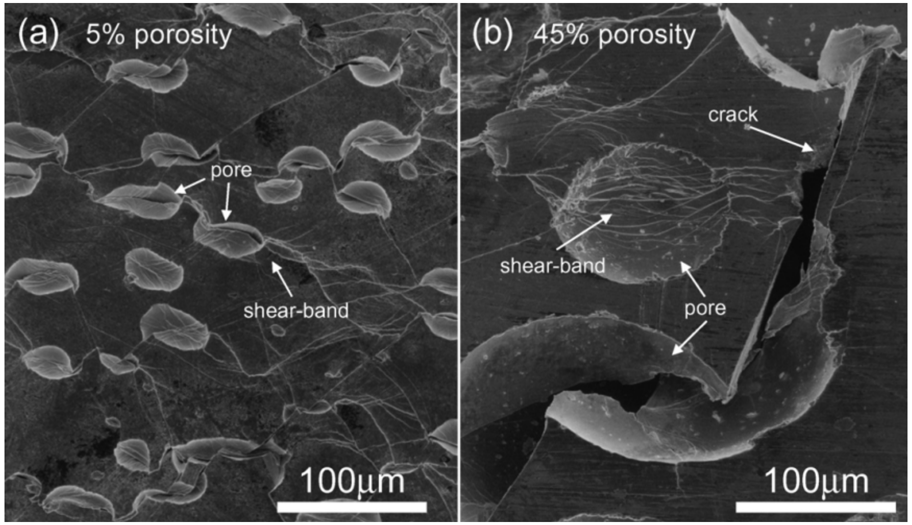

(a and b) SEM images of the surface structure of the porous $Pd_{35}Pt_{15}Cu_{30}P_{20}$ glassy alloy rods with porosities of 5 and 45% deformed up to strains of 0.2 and 0.05, respectively.

~65 vol%, 125-250 μm

(2004) foamed this alloy by the expansion of hydrogen bubbles precipitated from a supersaturated melt.

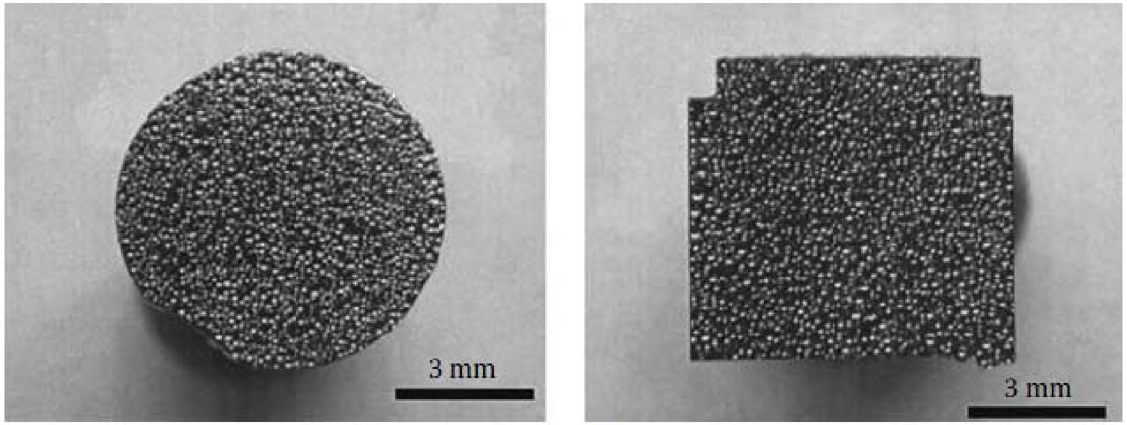

(a) (b)

FIGURE 4.16
(a) Transverse cross section and (b) longitudinal cross section of a 7mm diameter porous $Pd_{42.5}Cu_{30}Ni_{7.5}P_{20}$ alloy rod produced by melting the alloy for 10min at 813K under a hydrogen pressure of 1.5MPa and then water quenching. Note the uniformity of pore size in both the cross sections. (Reprinted from Wada, T. and Inoue, A., *Mater. Trans.*, 45, 2761, 2004. With permission.)

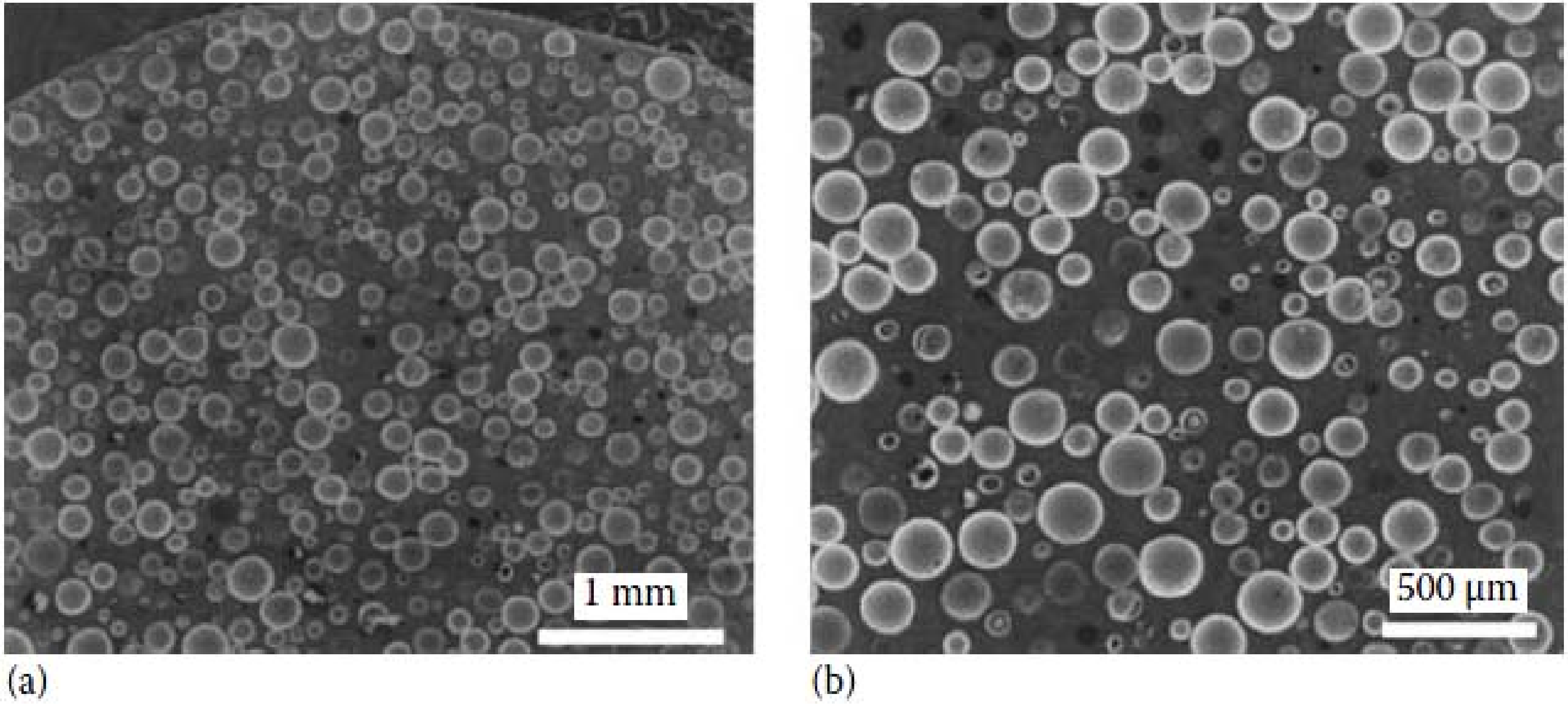

FIGURE 4.17
Scanning electron micrographs of the transverse cross section of the porous glassy $Pd_{42.5}Cu_{30}Ni_{7.5}P_{20}$ alloy rod quenched from 833 K under a hydrogen pressure of 1.5 MPa. The specimen was etched in concentrated H_2SO_4 solution for 3 h to reveal any contrast due to the presence of a crystalline phase. (a) Low-magnification and (b) high-magnification micrographs. Contrast due to the presence of a crystalline phase is not seen even in the high magnification micrograph. (Reprinted from Wada, T. and Inoue, A., *Mater. Trans.*, 45, 2761, 2004. With permission.)

Review of the state of the art in the processing of BMG foams III

- Brothers and Dunand (2004)
  the first amorphous foam using a commercial alloy, $Zr_{57}Nb_5Cu_{15.4}Ni_{12.6}Al_{10}$ (Vit106), which was produced by melt infiltration of beds of hollow carbon microspheres.

- (2005), Brothers et al
  demonstrated the use of the replication method for amorphous foams, in which liquid Vit106 was infiltrated into a packed bed of leachable BaF_2 salt particles that was removed after solidification in an acid bath.

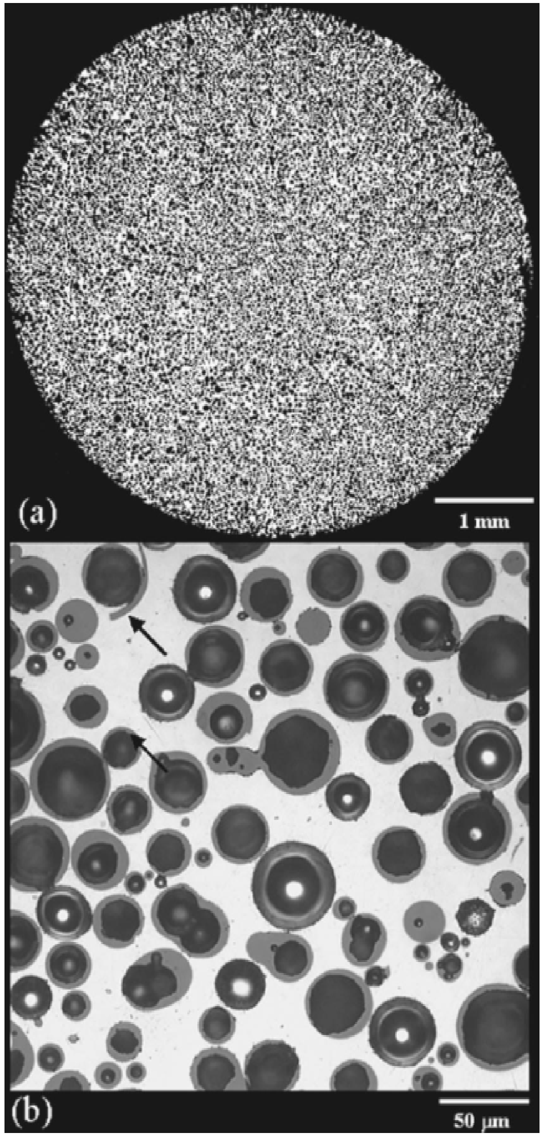

Optical micrographs showing the structure of syntactic Vit106 foam:
a) Low magnification image demonstrating foam uniformity;
b) Magnified image of the surface showing microscopic foam structure. Misshapen carbon microspheres are visible, as is a sphere wall fragment (indicated by Arrow). Good wetting is inferred from the lack of inter-particle porosity.

Review of the state of the art in the processing of BMG foams IV

Two other powder-based methods:

- (2006) Xie et al: reported amorphous $Zr_{55}Cu_{30}Al_{10}Ni_5$ with up to 67% porosity produced by partial spark-plasma consolidation of amorphous powders with diameters of 37–53 mm.

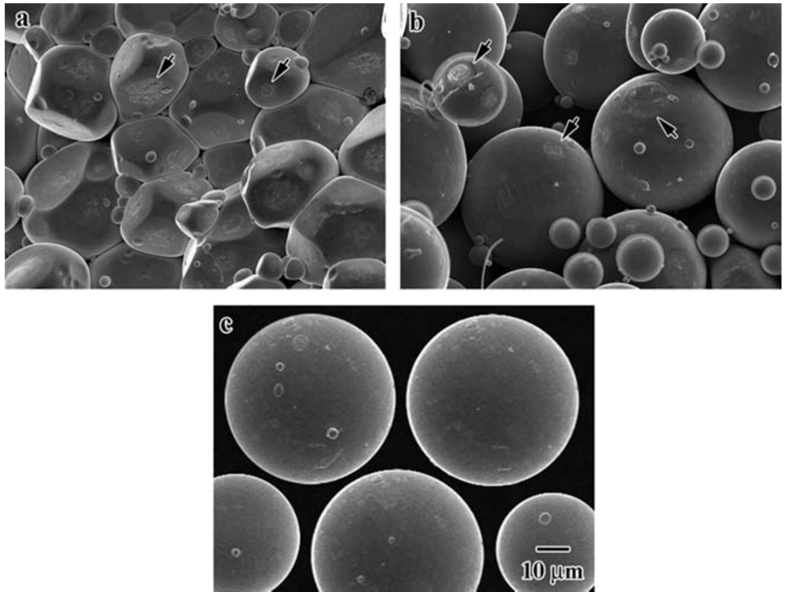

SEM micrographs of the transverse (mechanically crushed) cross section of the sintered porous $Zr_{55}Cu_{30}Al_{10}Ni_5$ bulk glassy alloys with porosities of 4.7% (a), 33.5% (b), and the original powder (c).

- Hasegawa et al studied the effects of lower levels (approximately 2%) of porosity retained in melt-spun ribbons of the same alloy, prepared from powder compacts containing aluminum nitride.

$AlN + Zr\ BMG \rightarrow ZrN + Zr\ BMG + N_2$ bubble

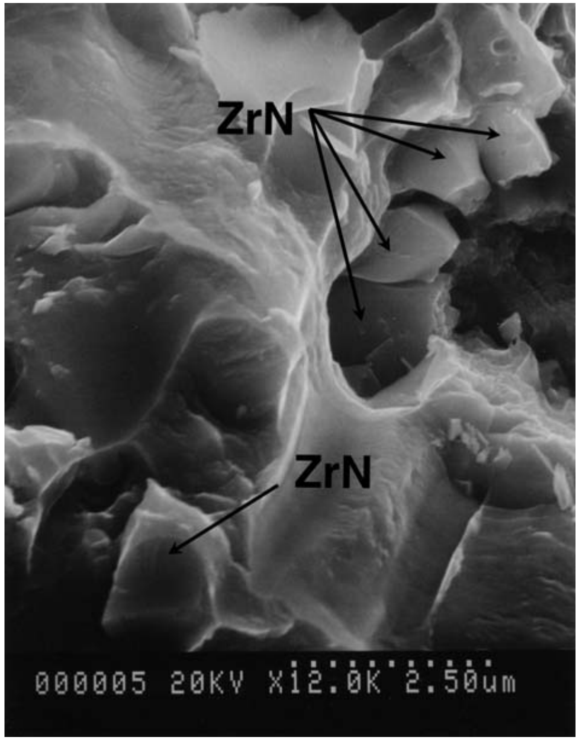

SEM image of the bending fracture surface of a glassy composite alloy ribbon. Synthesized ZrN is indicated by arrows.

Review of the state of the art in the processing of BMG foams V

- (2006), Jayaraj et al
  reported successful processing of nanoporous Ti-based amorphous metal ribbons using a method proposed in 2004 by Gebert et al. for a La-based metallic glass, in which one phase is selectively acid-leached from a two-phase amorphous metal.

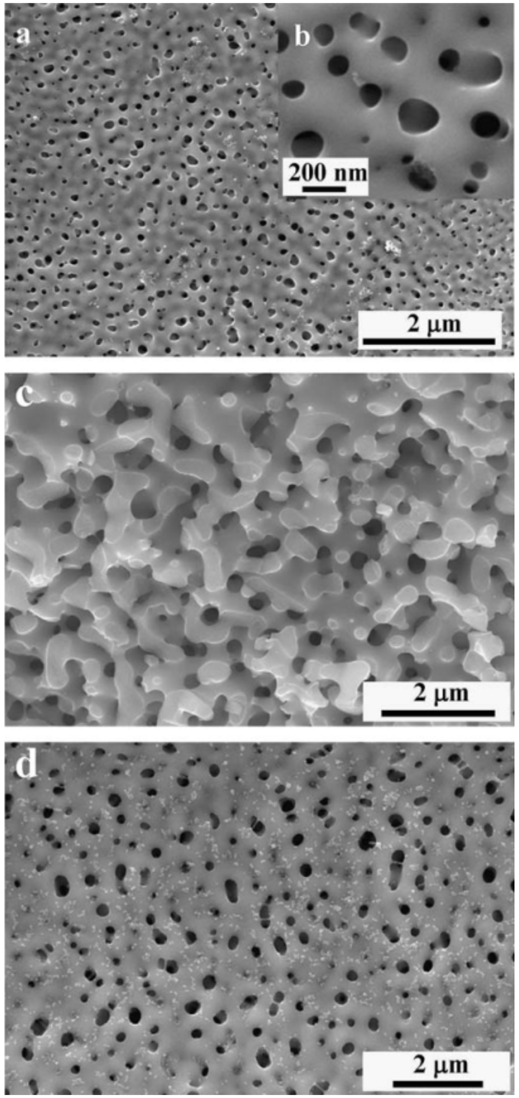

First nano prous amorphous metal
Fully interconnected porosity/ 15-155 nm

SEM images showing the formation of porous morphology of $Y_{20}Ti_{36}Al_{24}Co_{20}$ two-phase amorphous alloy. (a)–(c) Chemically dealloyed $Y_{20}Ti_{36}Al_{24}Co_{20}$ alloy in 0.1 M HNO_3 solution for 24 h:

(a) low magnification demonstrating pore formation;
(b) magnified image showing three-dimensionally connected open type pores;
(c) crosssection of the dealloyed ribbon specimen.
(d) Electrochemically dealloyed $Y_{20}Ti_{36}Al_{24}Co_{20}$ alloy in 0.1M HNO_3 solution with an applied voltage of 1.9 V for 30 min.

Review of the state of the art in the processing of BMG foams VI

- (2006) Lee and Sordelet

where the sacrificial phase is crystalline rather than amorphous, and the starting two phase material is formed by warm extrusion of powder blends rather than casting.

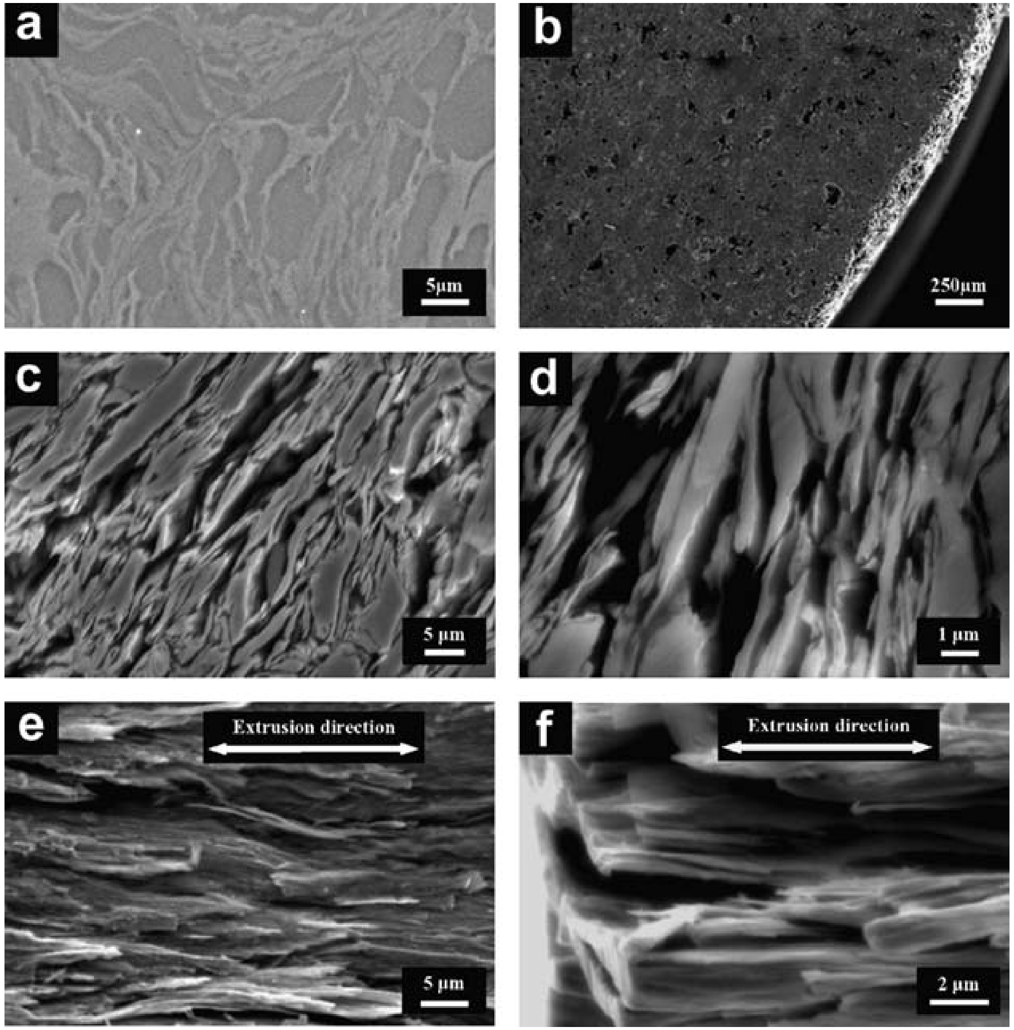

SEM images of porous $Cu_{47}Ti_{33}Zr_{11}Ni_8Si_1$ MG. Pores are uniformly distributed throughout the sample.

(a) Transverse polished cross section of $Cu_{47}Ti_{33}Zr_{11}Ni_8Si_1$ MG + Cu composite precursor before dissolution of the Cu;

(b) macrostructure of porous $Cu_{47}Ti_{33}Zr_{11}Ni_8Si_1$ MG;

(c) transverse cross-sectional microstructure of porous $Cu_{47}Ti_{33}Zr_{11}Ni_8Si_1$ MG;

(d) enlarged image of (c);

(e) longitudinal microstructure of porous $Cu_{47}Ti_{33}Zr_{11}Ni_8Si_1$ MG;

(f) detailed microstructure obtained from the lateral surface of the porous $Cu_{47}Ti_{33}Zr_{11}Ni_8Si_1$ MG.

Images of several representative porous amorphous metals, produced using liquid-state methods, are shown in Figure 1.
These methods demonstrated the possibility of foaming reactive Zr-based alloys of the sort used in most metallic glass applications.

Representative powder-processed porous amorphous metals are shown in Figure 2.

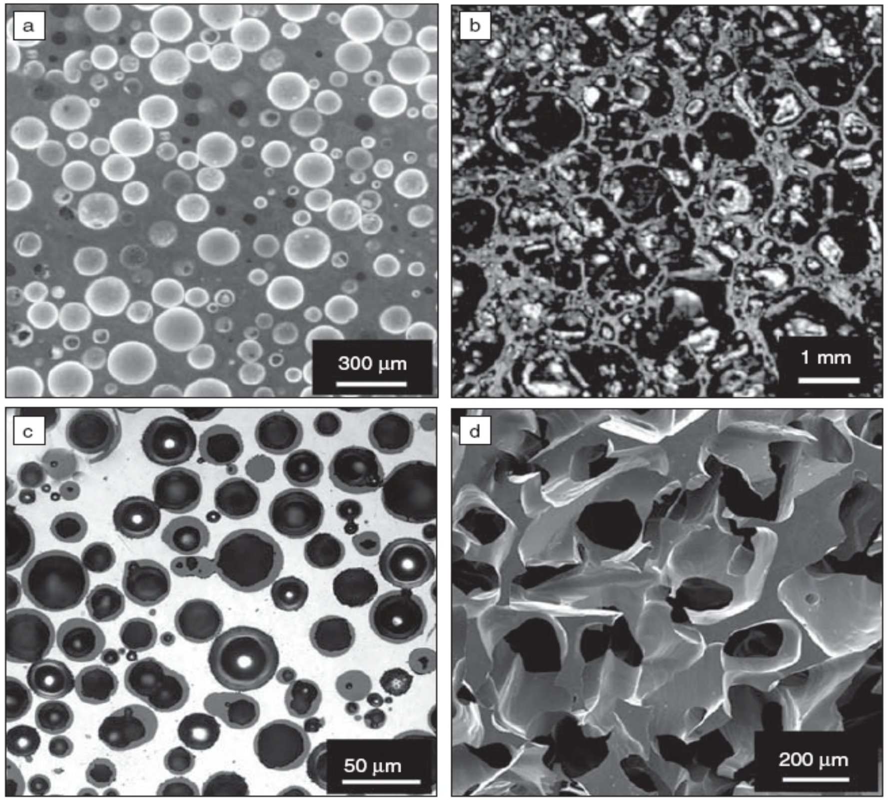

Figure 1. Examples of amorphous metal foams created by liquid-state and supercooled-liquid-state methods. (a) Pd-based foam (porosity $P = 42–46\%$) made by precipitation of dissolved hydrogen gas during cooling.[7] (b) Pd-based foam ($P = 85\%$) made by entrapping gas in the melt and then expanding it in the supercooled-liquid state.[5] (c) Zr-based foam made by infiltration of a bed of hollow carbon spheres. Volume fraction of spheres in the foam is 59%.[12] (d) Zr-based foam ($P = 78\%$) made by infiltration of BaF_2 salt particles followed by removal of those particles in an acid bath.[14]

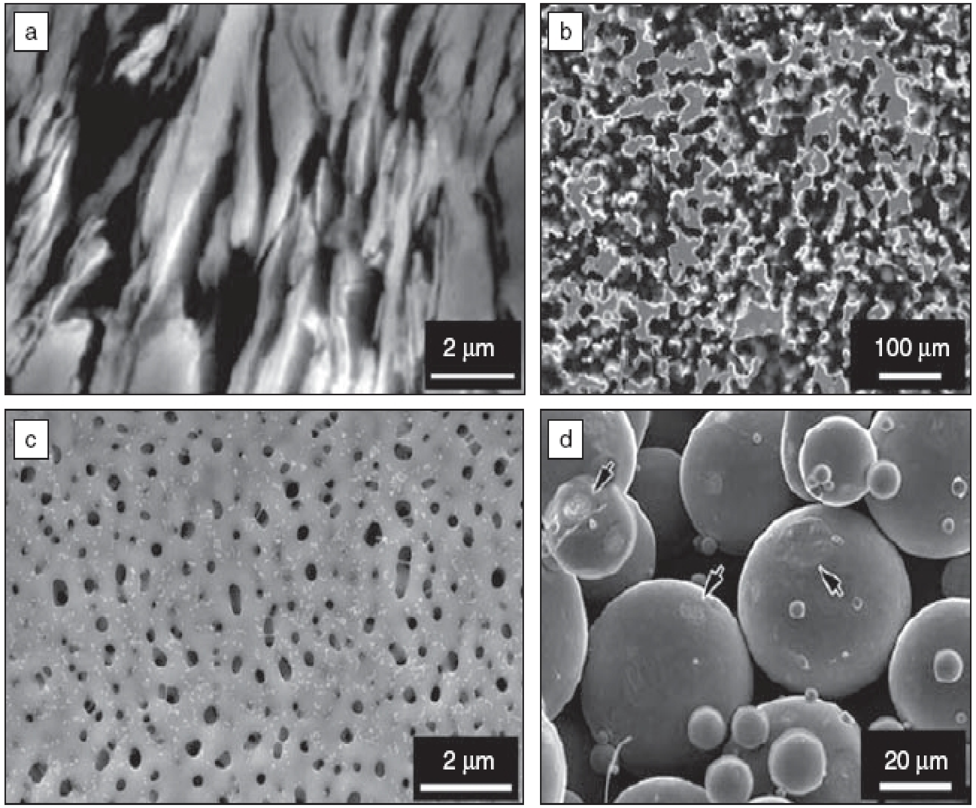

Figure 2. Examples of powder-processed porous amorphous metals and amorphous metal foams created by solid-state methods. (a) Cu-based foam (porosity $P = 75\%$) made by dissolution of crystalline Cu from an extruded composite.[21] (b) Ni-based foam ($P = 42\%$) made by dissolution of brass from an extruded composite.[22] (c) Ti-based porous amorphous metal (P not given) made by selective dissolution of one phase from a two-phase amorphous metal.[19] (d) Zr-based porous compact ($P = 34\%$) made by partial electroconsolidation of amorphous powders.[23]

Mechanical Properties (1)

The primary purpose of introducing porosity in amorphous metals is to hinder the propagation of shear bands.

Two main mechanisms of hindering shear-band propagation have been identified : shear-band disruption and shear-band stabilization.

i) shear-band disruption

→ (the same mechanisms active in amorphous metal-matrix composites) : Pores (like solid inclusions) interrupt shear bands when their paths intersect, favoring branching of those bands and/or nucleation of new bands.

ii) shear-band stabilization

→ (first noted during bending of thin amor. metal wires and foils)

a) each band relaxes the stress from a smaller volume of the surrounding glass, enabling a closer spacing of the neighboring shear bands subsequently initiated, thereby increasing band density and overall plastic strain.

b) shallower shear bands produce smaller shear offsets at the surfaces of the wires or foils, and these smaller offsets reduce the probability of nucleating a crack. In the case of Zr-based alloys, shear-band stabilization becomes noticeable for wire or foil thicknesses below about 1 mm.

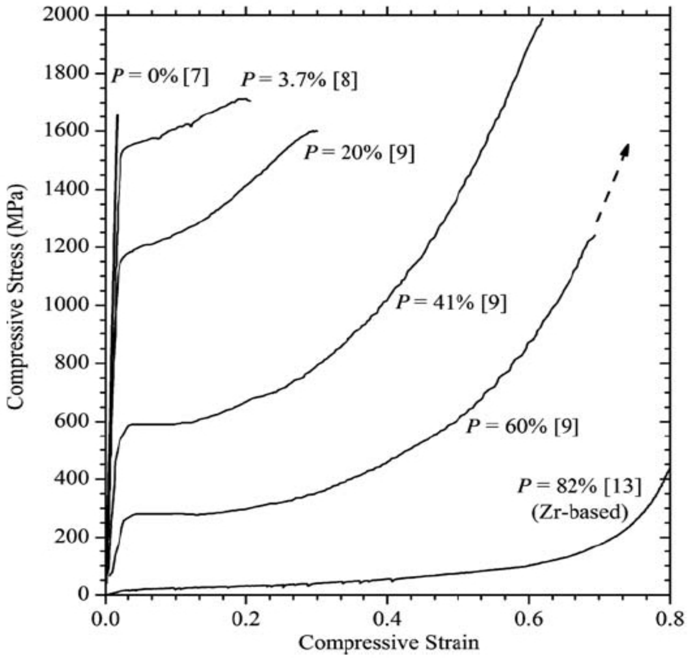

Figure 3. Compressive engineering stress–strain curves for several porous amorphous metals at intervals of approximately 20% porosity P. All but the highest-porosity material (which was processed from $Zr_{57}Nb_5Cu_{15.4}Ni_{12.6}Al_{10}$) were processed from $Pd_{42.5}Cu_{30}Ni_{7.5}P_{20}$.

The effectiveness of porosity in improving ductility and energy absorption in amor. metals, several compressive stress–strain curves for porous amorphous metals with porosities between 3.7% and 82% are shown in Figure

→ With increased porosity, the amorphous samples show decreasing strength and stiffness

Mechanical Properties(2)

A more comprehensive illustration of compressive ductility in porous amorphous metals is shown in Figure where failure strains are compiled as a function of porosity.

→ pore morphology & the effectiveness that determine the effectiveness of the ductilizing mechanisms_ some structures lead to almost no ductilization even at relatively high porosity.

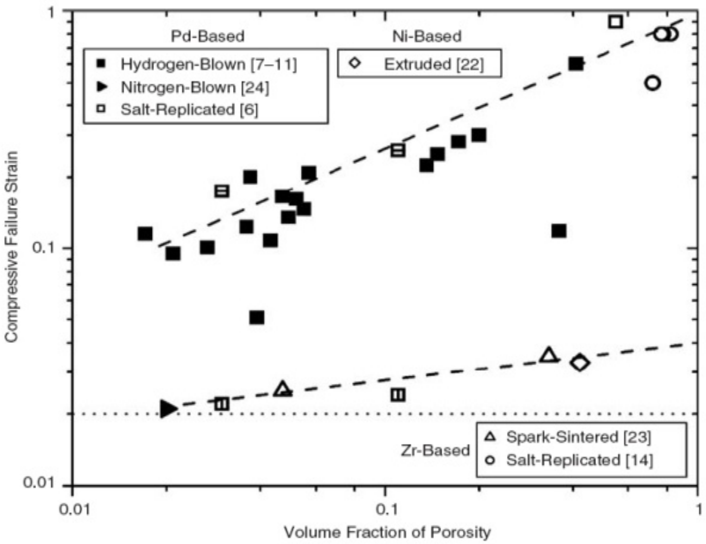

Figure 4. Compressive strain to failure as a function of porosity for published porous amorphous metals. Composition and processing methods are summarized in the labels. Open and solid symbols represent open-cell and closed-cell structures, respectively. Open squares with strikethroughs represent materials with elliptical porosity oriented parallel (vertical strikethroughs) and perpendicular (horizontal strikethroughs) to the loading axis.[9] The horizontal line at a failure strain of 2% is representative of fully dense amorphous metals.[1] The dashed lines are visual aids used to demonstrate how certain structures (upper line) produce substantial ductility, while others (lower line) produce less ductility.

Available data for the compressive yield strength and loading stiffness of porous amorphous metals are compiled in Figure

porous amorphous metals span a wide range of strengths, from less than 10 MPa for high-porosity foams to nearly 2 GPa for near-dense alloys.

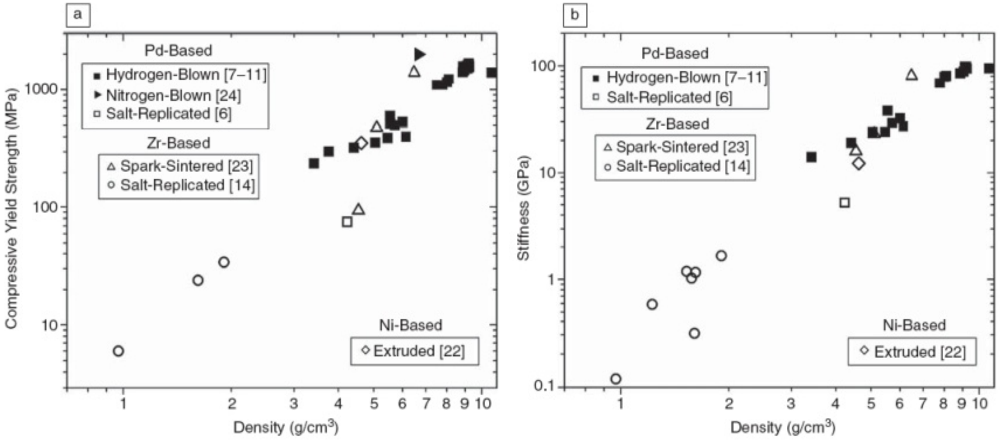

Figure 5. (a), (b) Compressive yield strength and stiffness as functions of density for published porous amorphous metals. Composition and processing methods are summarized in the labels. Open and solid symbols represent open-cell and closed-cell structures, respectively. Densities of the pore-free Zr-, Ni- and Pd-based glasses are 6.8 g/cm³, 7.9 g/cm³, and 9.4 g/cm³, respectively.

Applications

- Porosity can be used as a means of selectively and continuously trading strength and stiffness for ductility, weight reduction, and energy absorption

↔

- Porous amorphous metals could find use in a variety of applications, from structural materials to energy absorption or packaging applications

High strength & compressive application
→ only small relative losses in strength

At larger porosities, better energy absorption capacity, when compared on a volumetric basis, than crystalline Al-based foams

- The intrinsic benefits of AM
  →Large elastic energy return, wear resistance, and corrosion resistance and so on.
- Limitation
  → Low tensile ductility, cooling rate, high costs
- Unknown
  → Resistance to fatigue and tensile fracture

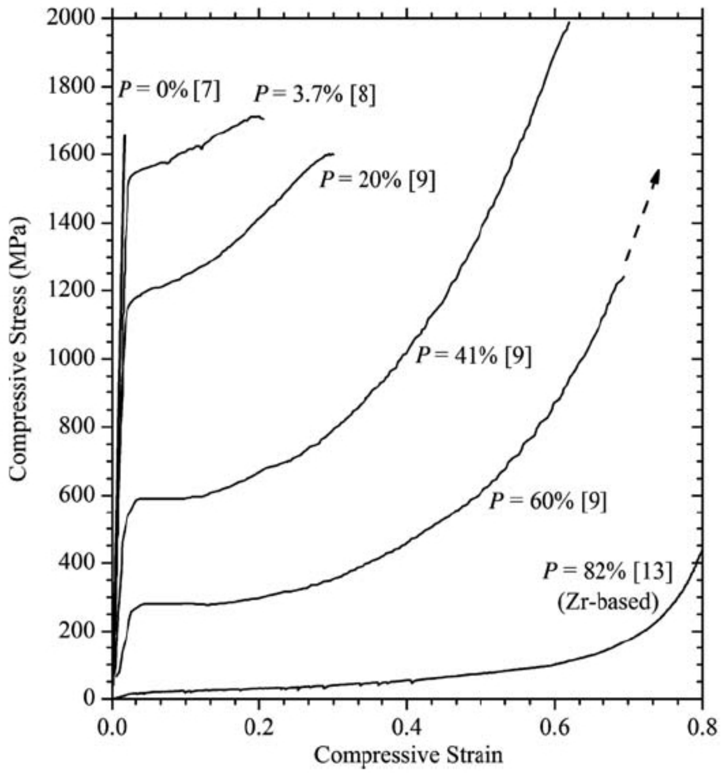

Figure 3. Compressive engineering stress–strain curves for several porous amorphous metals at intervals of approximately 20% porosity *P*. All but the highest-porosity material (which was processed from $Zr_{57}Nb_5Cu_{15.4}Ni_{12.6}Al_{10}$) were processed from $Pd_{42.5}Cu_{30}Ni_{7.5}P_{20}$.

Conclusions

Porous amorphous metals represent a promising new step toward the engineering application of amorphous metals by enabling mechanical properties and density to be varied across a wider range than is possible using monolithic alloys or composites.

- compressive failure strains
  → can be varied from near-maximum values
- compressive strength and stiffness
  → can be varied from ~2% to more than 80%

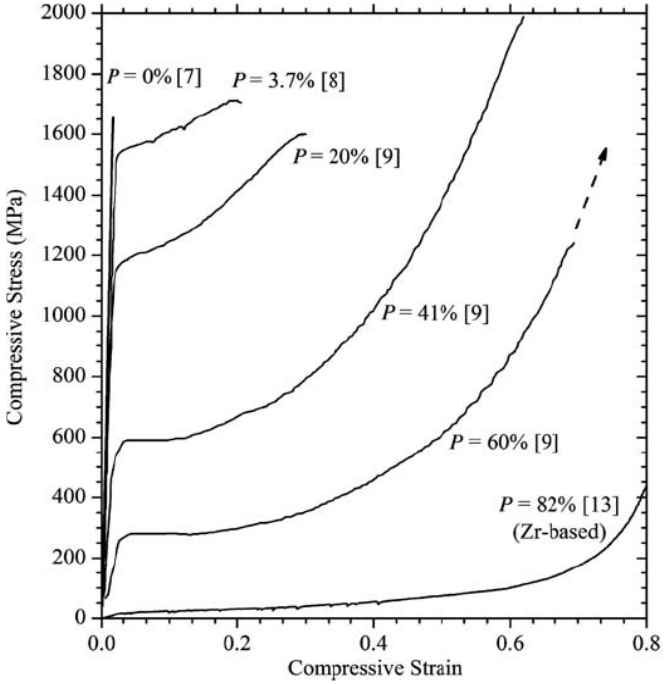

Figure 3. Compressive engineering stress–strain curves for several porous amorphous metals at intervals of approximately 20% porosity P. All but the highest-porosity material (which was processed from $Zr_{57}Nb_5Cu_{15.4}Ni_{12.6}Al_{10}$) were processed from $Pd_{42.5}Cu_{30}Ni_{7.5}P_{20}$.

Porosity introduction can optimize density-compensated mechanical properties and tailor other properties such as fluid permeability, specific surface area, and acoustic damping.